Applied Catalysis B: Environmental 327 (2023) 122432

Contents lists available at ScienceDirect

Applied Catalysis B: Environmental

journal homepage: www.elsevier.com/locate/apcatb

Direct photoconversion of nitrite to dinitrogen on Pd/TiO_2 coupled with photooxidation of aquatic pollutants

Shinbi Lee [a], Yoojin Lee [b], Wonyong Choi [a,*]

[a] KENTECH Institute for Environmental and Climate Technology, Korea Institute of Energy Technology (KENTECH), Naju 58330, South Korea
[b] Division of Environmental Science and Engineering, Pohang University of Science and Technology (POSTECH), Pohang 37673, South Korea

ARTICLE INFO

Keywords:
Photocatalysis
Titania
Nitrite reduction
Solar water treatment
Denitrification

ABSTRACT

Nitrate (NO_3^-) and nitrite (NO_2^-) are ubiquitous aquatic pollutants and should be controlled for water quality. Although diverse methods of nitrate/nitrite reduction have been developed, most require chemical reductants and external energy inputs. Nitrite is oxidized by photogenerated hydroxyl radicals (•OH) in an aqueous suspension of Pd-loaded TiO_2 (Pd/TiO_2) with producing nitrate as a major product. The main photoconversion product of nitrite is changed from nitrate to N_2 on Pd/TiO_2 in the presence of aquatic pollutants (arsenite (As(III)) or 4-chlorophenol (4-CP)) which can suppress the photooxidation of NO_2^- by scavenging holes/•OH. The photogenerated H_2 on Pd/TiO_2 serves as a main reductant and was immediately consumed for reducing nitrite to N_2. The presence of As(III) or 4-CP also enhanced the durability of Pd/TiO_2 by efficiently scavenging hole/•OH that may oxidize Pd nanoparticles. The proposed process can be a viable treatment option for nitrite-contaminated water containing various aquatic pollutants.

1. Introduction

As a high load of fertilizers and nitrogenous chemicals are being consumed [1,2], surplus nitrogen species such as ammonia and organic nitrogen compounds are oxidized to nitrate (NO_3^-) and nitrite (NO_2^-) which are accumulated in the environment due to the imbalance between anthropogenic discharge and natural removal processes [3,4]. Excessive nitrogen load in water induces the overgrowth of aquatic plants and microorganisms, which is regarded as a major cause of eutrophication [5]. In particular, the accumulation of nitrate leads to the generation of nitrite, a toxic intermediate, *via in vivo* reduction in microorganisms [6,7] or during the nitrate removal processes [8,9]. Nitrite is difficult to be controlled due to its instability and unpredictable reactions with other matters in water. Therefore, the complete understanding of its transformation behavior in the remediation process is essential for the effective control of nitrite.

Several technologies such as biological denitrification [10] and (electro)catalytic process [11–13] have been developed for converting nitrate and/or nitrite to harmless N_2. In this system, nitrate (or nitrite) can be converted to N_2 through sequential steps of reduction ($NO_3^- \rightarrow NO_2^- \rightarrow NO \rightarrow N_2O \rightarrow N_2$) *via* multi-electron transfers to achieve high N_2 selectivity. In particular, elaborate designing of (electro)catalysts (*e.g.*, bimetallic alloy [14], oxo-molybdenum sulfide electrocatalyst [15], and metal/carbon composite [16]) enables the selective conversion of nitrite to N_2 by precisely controlling active catalytic sites. However, the electrocatalytic systems suffer from some intrinsic demerits such as the need of supporting electrolytes that should be removed from the treated water, the consumption of electrical power, and the operation at alkaline or acidic pH condition (not circumneutral) [17,18].

As a suitable alternative for nitrite removal, photocatalytic denitrification has been investigated to overcome the demerits of the conventional methods [19–23]. The photocatalytic process can operate under circumneutral ambient condition without the need of electricity and chemicals as long as suitable photons are available. For the nitrite/nitrate removal, the photocatalyst is typically composed of metal oxide semiconductor and mono/bimetallic cocatalyst [24–26]. For the efficient conversion of nitrite to N_2, the metal catalyst should have not only high adsorption affinity for nitrite but also high hydrogen spill-over activity [27]. Among various metallic cocatalysts, palladium (Pd) has been studied as a superior metal cocatalyst for converting nitrite to N_2 selectively, but high conversion efficiency of nitrite to N_2 was observed only in the presence of H_2 or organic electron donors even on Pd catalyst [28–31]. A recent study successfully demonstrated the performance of the ternary composite photocatalyst of Cu-Pd/rGO/TiO_2 that directly

* Corresponding author.
E-mail address: wchoi@kentech.ac.kr (W. Choi).

https://doi.org/10.1016/j.apcatb.2023.122432
Received 28 October 2022; Received in revised form 31 December 2022; Accepted 2 February 2023
Available online 3 February 2023

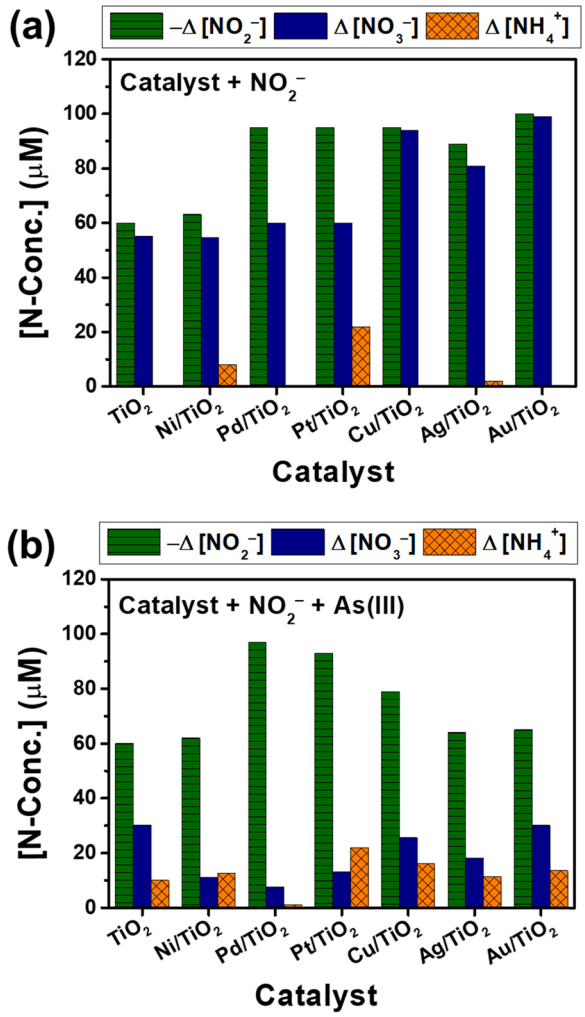

Fig. 1. The nitrite removal and N-products distribution after 2 h photocatalytic conversion of NO_2^- in aqueous suspension of bare and metal-loaded TiO_2 particles (a) in the absence of and (b) in the presence of As(III) as an aquatic pollant. (Metal content: 1 wt%; [catalyst] = 0.5 g/L; $[NO_2^-]_0$ = 100 μM; [As (III)]$_0$ = 100 μM (for b); pH = 5.3–5.7 (not adjusted); initially Ar-purged (de-aerated suspension); λ > 320 nm irradiation).

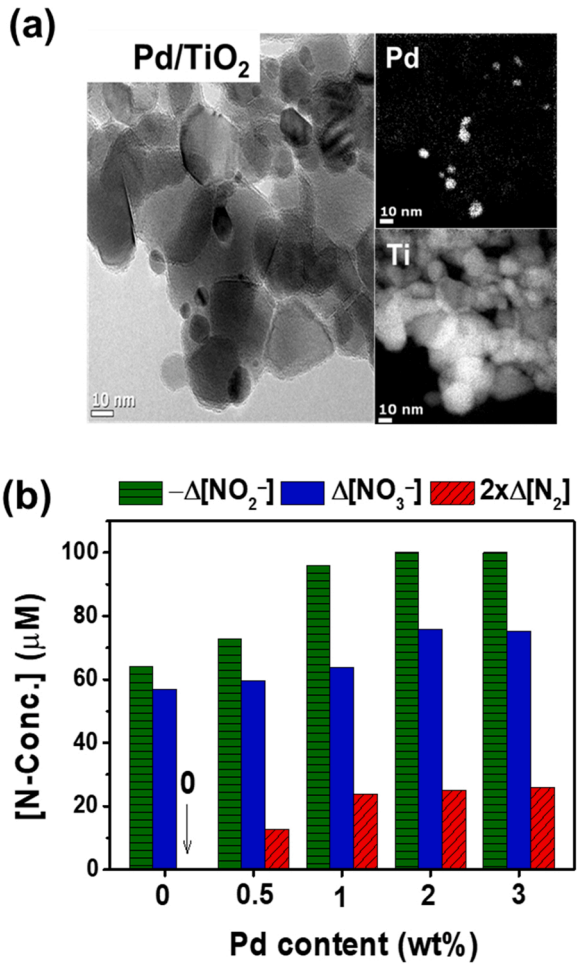

Fig. 2. (a) TEM image of Pd(1 wt%)/TiO_2 and the energy-filtered TEM (EFTEM) of Pd and Ti. (b) The nitrite removal and N-products distribution after 2 h photocatalytic conversion of NO_2^- on Pd/TiO_2 with different Pd content. ([catalyst] = 0.5 g/L; $[NO_2^-]_0$ = 100 μM; pH = 5.3–5.7 (not adjusted); initially Ar-purged (de-aerated suspension); λ > 320 nm irradiation).

convert nitrite to N_2 without the need of external electron donors but the co-presence of all three components (Cu, Pd, rGO) is essentially needed to achieve the direct photoconversion to N_2 [32]. Although the presence of Pd component should play the key role in the conversion of nitrite to N_2 [33,34], Pd/TiO_2 alone is inefficient for the photoconversion of nitrite to N_2 and requires additional H_2 or organic electron donor as a reductant of nitrite (Eqs. 1,2).

$$2NO_2^- + 8\,H^+ + 6e^- \rightarrow N_2 + 4\,H_2O \quad (1)$$

$$2NO_2^- + 3\,H_2 \rightarrow N_2 + 2\,H_2O + 2OH^- \quad (2)$$

Therefore, cost-efficient and scalable applications of the photocatalytic system for the nitrite removal are still not feasible because of the low conversion efficiency without external electron donors [26]. From the practical point of view, it should be noted that the real nitrite-contaminated water always contains various aquatic pollutants but their effects on the nitrite conversion mechanism were little investigated. In the photocatalytic system for the direct conversion of NO_2^- to N_2, the effects of various aquatic pollutants have not been systematically studied.

In this study, we investigated the photocatalytic reduction of NO_2^- to N_2 on Pd/TiO_2 that is directly coupled with the photooxidation of

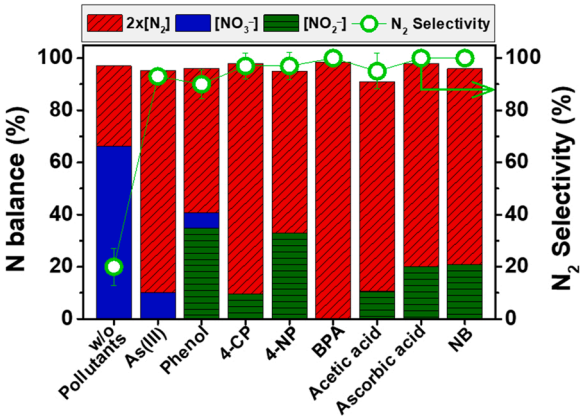

Fig. 3. The N-products distribution and the total nitrogen (TN) balance after 2 h photocatalytic conversion of NO_2^- in the Pd/TiO_2 suspension containing various pollutants. ([Pd/TiO_2] = 0.5 g/L; Pd content of 1 wt%; $[NO_2^-]_0$ = [Pollutant]$_0$ = 300 μM; pH = 5.3–6.5 (not adjusted); initially Ar-purged (de-aerated suspension); λ > 320 nm irradiation).

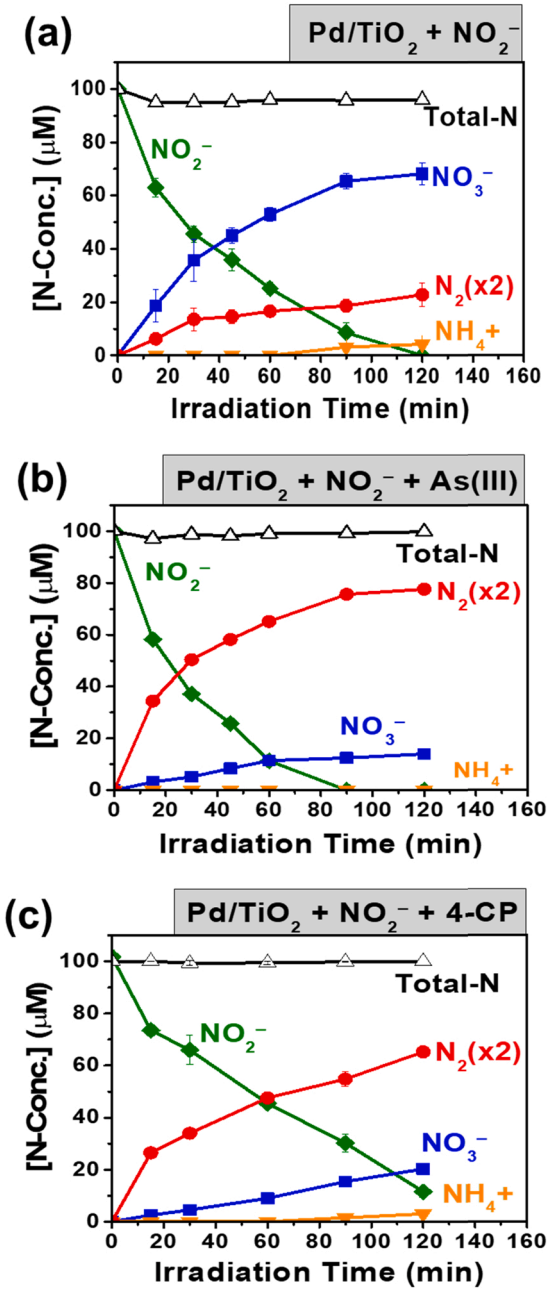

Fig. 4. Time profiles of the photocatalytic removal of NO_2^- and the concurrent generation of NO_3^-, N_2 and NH_4^+ in the aqueous suspension of Pd/TiO_2 containing (a) no pollutants, (b) As(III) (100 μM), and (c) 4-CP (100 μM). ([Pd/TiO_2] = 0.5 g/L; Pd content of 1 wt%; $[NO_2^-]_0$ = 100 μM; pH = 5.3–6.1 (not adjusted); initially Ar-purged (de-aerated suspension); λ > 320 nm). The dissolved N_2 concentration in the suspension should be negligibly small according to the Henry's law constant of N_2 (<2% of N_2 gas in the headspace, smaller than the experimental uncertainty in the measured N_2 gas amount) and was neglected in the total N balance calculation.

various aquatic pollutants. The coupled photocatalytic reactions were tested in a single batch reactor that operated without the need of chemical reductants and external energy input except light. We investigated and discussed (i) the role of the Pd on TiO_2 for nitrite photoconversion, (ii) the effects of *in-situ* generated hydroxyl radicals and H_2 on Pd/TiO_2 on the N_2 selectivity, (iii) the detailed mechanisms of the reaction with hydroxyl radicals (•OH) and NO_2^-/NO_3^-, and (iv) the effect of various aquatic pollutants on suppressing the nitrate generation and enhancing the N_2 selectivity and the photostability of Pd/TiO_2.

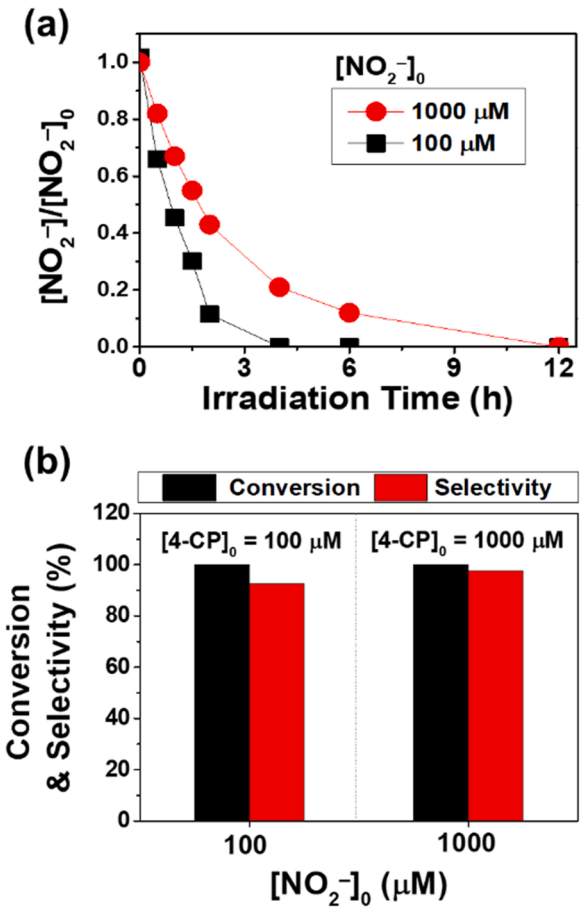

Fig. 5. Comparison of the photocatalytic removal of nitrite at different concentrations (100 *vs.* 1000 μM) in the suspension of Pd/TiO_2. (a) The time profiles of nitrite removal in the presence of 4-CP ($[NO_2^-]$: [4-CP] =1: 1) and (b) the nitrite conversion and the selectivity to N_2 after 12 h photoreaction ([catalyst] = 0.5 g/L; Pd content of 1 wt%; pH = 5.3–6.1 (not adjusted); initially Ar-purged (de-aerated suspension); λ > 320 nm).

2. Methods

2.1. Catalysts preparation and characterizations

M/TiO_2 (M= Ni, Pd, Pt, Cu, Ag, Au) was prepared using an *in-situ* photodeposition method. $NiCl_2$, $PdCl_2$, H_2PtCl_6•xH_2O, $CuCl_2$, $AgNO_3$ and $AuCl_2$ (Aldrich) were used as metal precursors. TiO_2 (P25) was suspended in an aqueous solution containing methanol (4%, v/v) as a hole scavenger and then a calculated amount of metal precursor was added. The resulting suspension was subsequently irradiated to deposit metal nanoparticles on TiO_2 under UV light for 1 h using a 300-W mercury lamp. The irradiated suspension was filtered to recover the metal-loaded TiO_2 powder, washed with distilled water, and dried under air. To estimate the amount of photodeposited metal (Ni, Pd, Pt, Cu, Ag, Au), the residual amounts of metal precursors after photodeposition were measured using an inductively coupled plasma optical emission spectrometer (ICP-OES-6300-Thermo Scientific). The residual concentration of each metal precursor after 1 h photodeposition was negligible, which indicated that each metal precursor was quantitatively deposited on TiO_2.

High-resolution transmission electron microscopy (HR-TEM) and electron energy-loss spectroscopy (EELS) were carried out using a JEOL JEM-2100FS with image Cs-corrector (200 keV) to analyze the Pd-loaded TiO_2. X-ray photoelectron spectroscopy (XPS) was performed using Axis Ultra DLD spectrometer (Kratos Inc) employing a monochromatic Al Kα X-ray source.

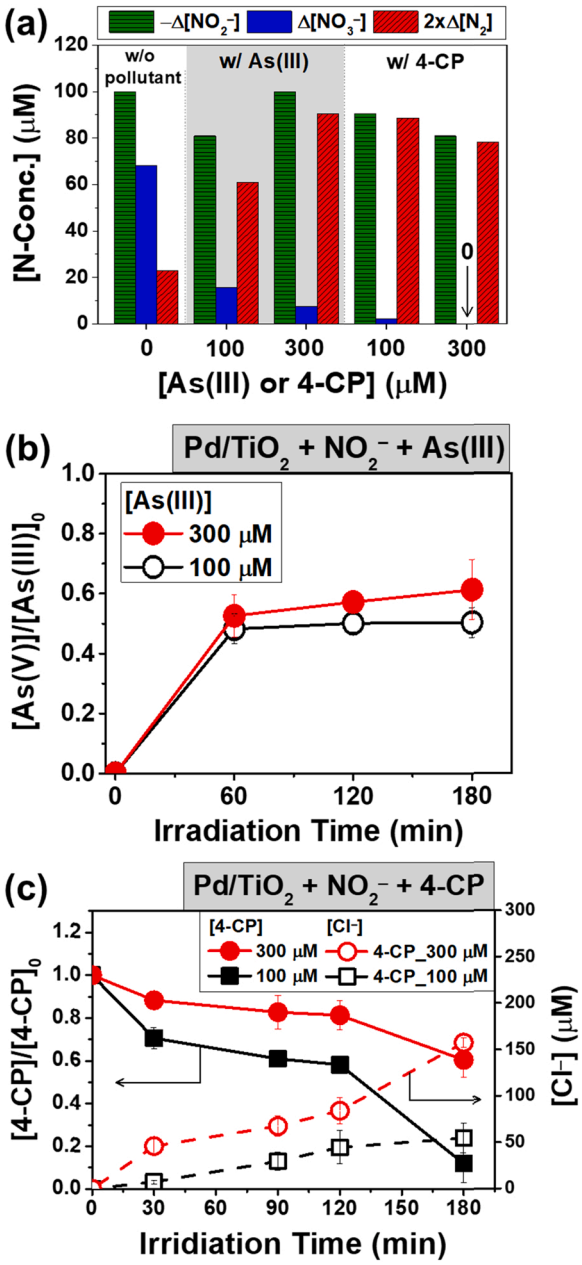

Fig. 6. (a) The nitrite removal/N-products distribution and the total nitrogen (TN) balance after 3 h photocatalytic reaction in the presence of As(III) or 4-CP at 0, 100, and 300 μM. Time profiles of the photocatalytic (b) oxidation of As (III) to As(V) and (c) degradation of 4-CP (along with the concurrent chloride generation). ([catalyst] = 0.5 g/L; Pd content of 1 wt%; $[NO_2^-]_0$ = 100 μM; pH = 5.3–6.1 (not adjusted); initially Ar-purged (de-aerated suspension); λ > 320 nm).

2.2. Photocatalytic reaction

A quartz reactor (55.7 mL) was used to carry out the photocatalytic reactions. A proper amount of catalyst powder was dispersed in deionized water (0.5 g/L) and an aliquot of nitrite stock solution ($NaNO_2$, Sigma) was subsequently added to the suspension to set an initial nitrite concentration. The solution was then sonicated for 1 min to ensure the dispersion of TiO_2 particles. The reactor was sealed with a rubber septum and Ar gas was purged through the rubber septum for 30 min before light irradiation. The irradiation from a 300-W Xenon arc lamp (Oriel) was filtered using a long-pass filter (λ > 320 nm) and a 10-cm IR water filter, and then focused onto the reactor. For recycling tests of the

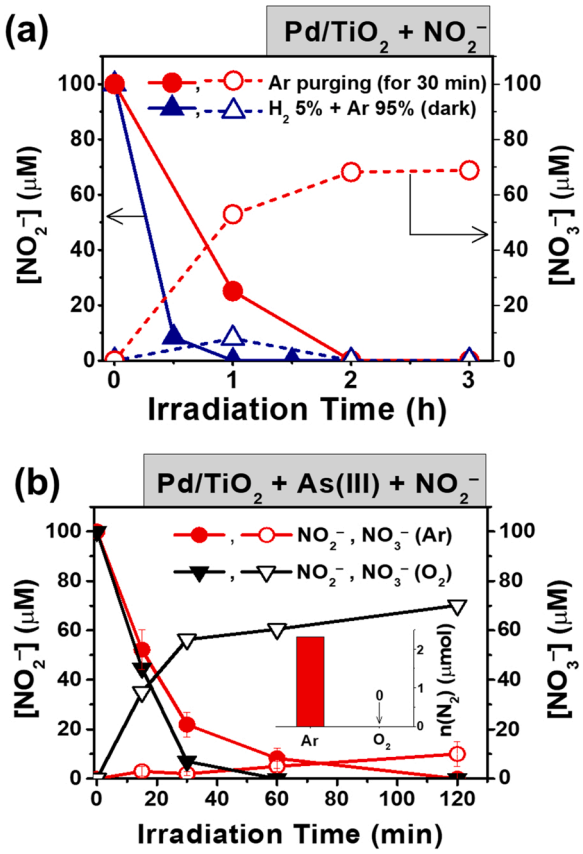

Fig. 7. (a) Time profiles of the photocatalytic removal of NO_2^- (filled symbols) and the concurrent generation of NO_3^- (open symbols) under different gas purging conditions. The dark catalytic conversion of nitrite on Pd/TiO_2 in the presence of H_2 gas is compared as well. (b) The same time profiles in the presence of As(III) under different gas purging conditions. (Inset: Total amount of photogenerated N_2 after 2 h reaction at different purging conditions.) ([catalyst] = 0.5 g/L; Pd content: 1 wt%; $[NO_2^-]_0$ = [As(III)]$_0$ = 100 μM; pH = 5.3–5.7 (not adjusted); initially Ar- or O_2 purged; λ > 320 nm).

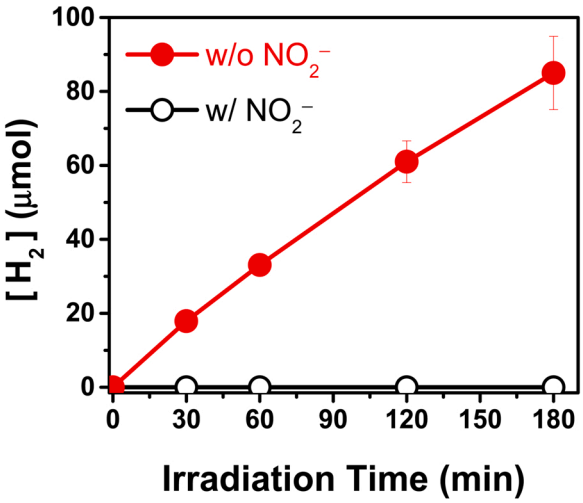

Fig. 8. Time profiles of the photocatalytic H_2 evolution on Pd/TiO_2 with or without NO_2^-. ([catalyst] = 0.5 g/L; Pd content: 1 wt%; $[NO_2^-]_0$ = 100 μM; pH = 5.3–6.1 (not adjusted); initially Ar-purged (de-aerated suspension); λ > 320 nm).

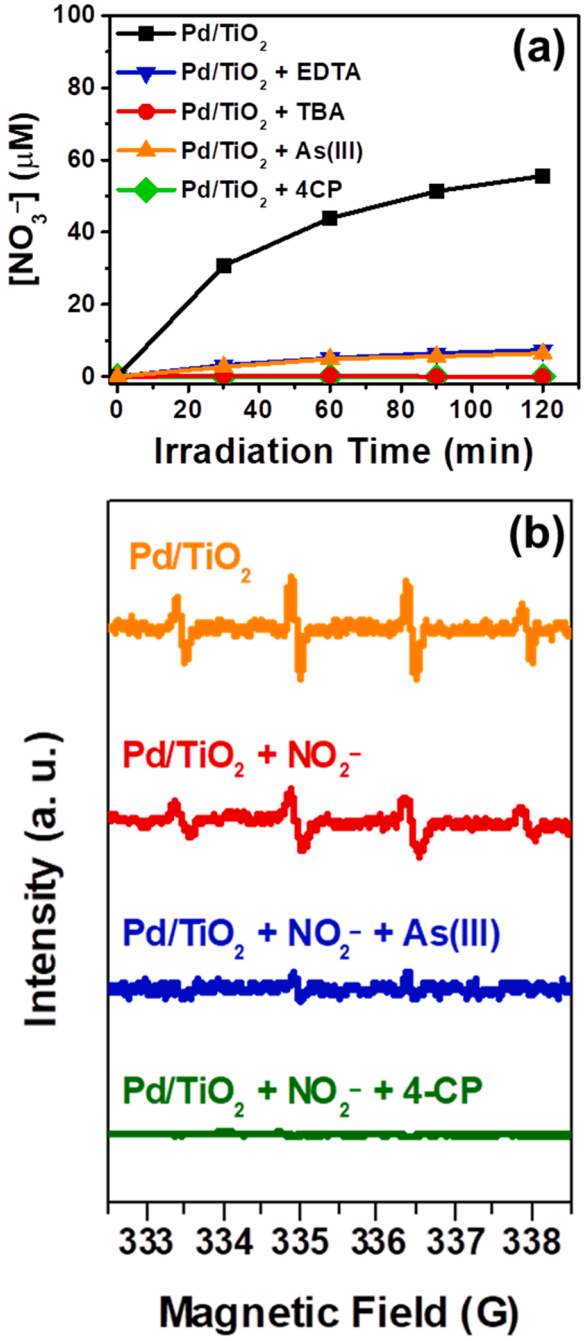

Fig. 9. (a) The effects of TBA, EDTA, As(III) and 4-CP addition on the photocatalytic oxidation of NO_2^- to NO_3^-. (Pd content: 1 wt%; $[NO_2^-]_0$ = 100 μM; [catalyst] = 0.5 g/L; $[As(III)]_0$ = $[4\text{-CP}]_0$ = 300 μM; $[TBA]_0$ = $[EDTA]_0$ = 500 mM; pH = 5.3–6.5 (not adjusted); initially Ar-purged (de-aerated suspension); λ > 320 nm) (b) EPR spectra of OH-DMPO adduct formed in the irradiated Pd/TiO_2 suspension. ($[NO_2^-]_0$ = $[As(III)]_0$ = $[4\text{-CP}]_0$ = 300 μM; $[DMPO]_0$ = 10 mM; Other conditions are the same as (a)).

photocatalyst, the suspension was filtered to recover the catalyst after the photoreaction. The collected catalyst was washed and then re-dispersed in a fresh substrate solution. This procedure was repeated for 5 cycles.

2.3. Analysis of reactants and products

Sample aliquots were withdrawn by a 1 mL syringe intermittently during the photoreaction, and the catalyst was filtered before the analysis. The analysis of Cl^-, NO_3^-, NO_2^-, and NH_4^+ was performed using an ion chromatograph (IC: Dionex DX-120) equipped with a conductivity detector and AS-14 column for anions and CS-14 column for cations. Total nitrogen (TN) was measured using TN reagent kits (Hach, Loveland, CA). The amounts photocatalytic generation of N_2 and H_2 gas were measured using a Shimadzu GC-8A gas chromatograph (GC) equipped with a thermal conductivity detector (TCD) and a 5-Å molecular sieve column. Argon was used as a carrier gas. Gaseous samples were collected from the headspace of the reactor by a gas-tight syringe and then injected manually into the GC to analyze H_2 and N_2. The conversion of nitrite and the N_2 selectivity were calculated using the following equations:

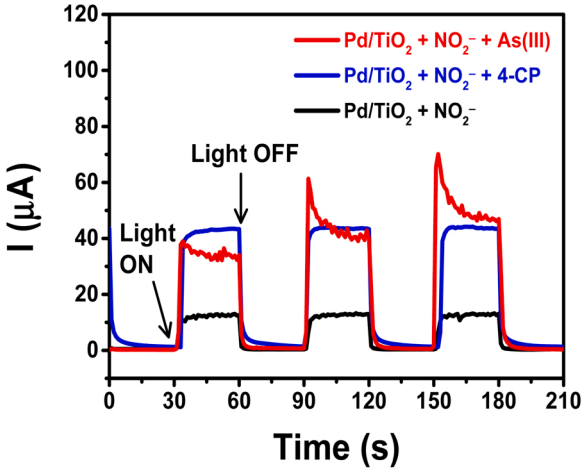

Fig. 10. Time profiles of the photocurrent generation on the Pd/TiO_2 electrode in the presence of NO_2^-, 4-CP, and As(III) before, during, and after UV irradiation. (Pd content: 1 wt%; $[NaClO_4]$ = 0.1 M; $[NO_2^-]_0$ = $[4\text{-CP}]_0$ = $[As(III)]_0$ = 1 mM; pH_i = 3 (adjusted by $HClO_4$); continuously Ar purged; λ > 320 nm).

$$\text{Conversion } (\%) = ([NO_2^-]_0 - [NO_2^-]_t)/[NO_2^-]_0 \text{ x } 100 \quad (3)$$

$$\text{Selectivity } (\%) = 2[N_2]/([NO_2^-]_0 - [NO_2^-]_t) \text{ x } 100 \quad (4)$$

The concentrations of organic pollutants (Phenol, 4-Chlorophenol (4-CP), 4-Nitrophenol (4-NP), Bisphenol A (BPA), Acetic acid, Ascorbic acid, Nitrobenzene (NB)) were quantitatively analyzed using a high-performance liquid chromatograph (Agilent 1260 Infinity) equipped with a diode array detector and a ZORBAX 300SB-C18 column.

The concentration of photogenerated As(V) was colorimetrically determined using a molybdenum blue method with a detection limit of 0.8 μM in which arsenomolybdate is reduced with ascorbic acid to form an intensively blue complex [35]. A solution of 0.1 mL of ascorbic acid and 0.2 mL of molybdate reagent solution were mixed with 4 mL sample solution (diluted 4-fold with deionized water) in a conical tube. After 2 h of color development, the concentration of As(V) was estimated by measuring the absorbance at 870 nm (ε = 19550 $M^{-1}cm^{-1}$) using a UV−visible spectrophotometer (Libra S22, Biochrom).

As for the experiments with lower As(III) concentrations, the quantitative analysis of As(V) was performed by IC using a Dionex ICS-2100 (Dionex IonPac AS18 (4 × 250 mm) column with a conductivity detector, 39 mM KOH eluent). For the analysis of residual As(III), the sample was allowed to pass through a silica-based anion exchange cartridge (LC-SAX SPE Tube, supelco), which can hold As(V), so that As(III) only can be collected in the effluent solution. The effluent was analyzed to measure the concentration of As(III) by ICP-AES (Iris Advantage).

For electron paramagnetic resonance (EPR) analysis for •OH detection, 5,5-dimethyl-1-pyrroline N-oxide (DMPO, Sigma) was used as a spin trapping agent. The EPR signals of the DMPO−OH spin adduct were monitored using an EPR spectrometer (JES-X310, Jeol Co.) under the following conditions: microwave power of 1.00 mW, microwave

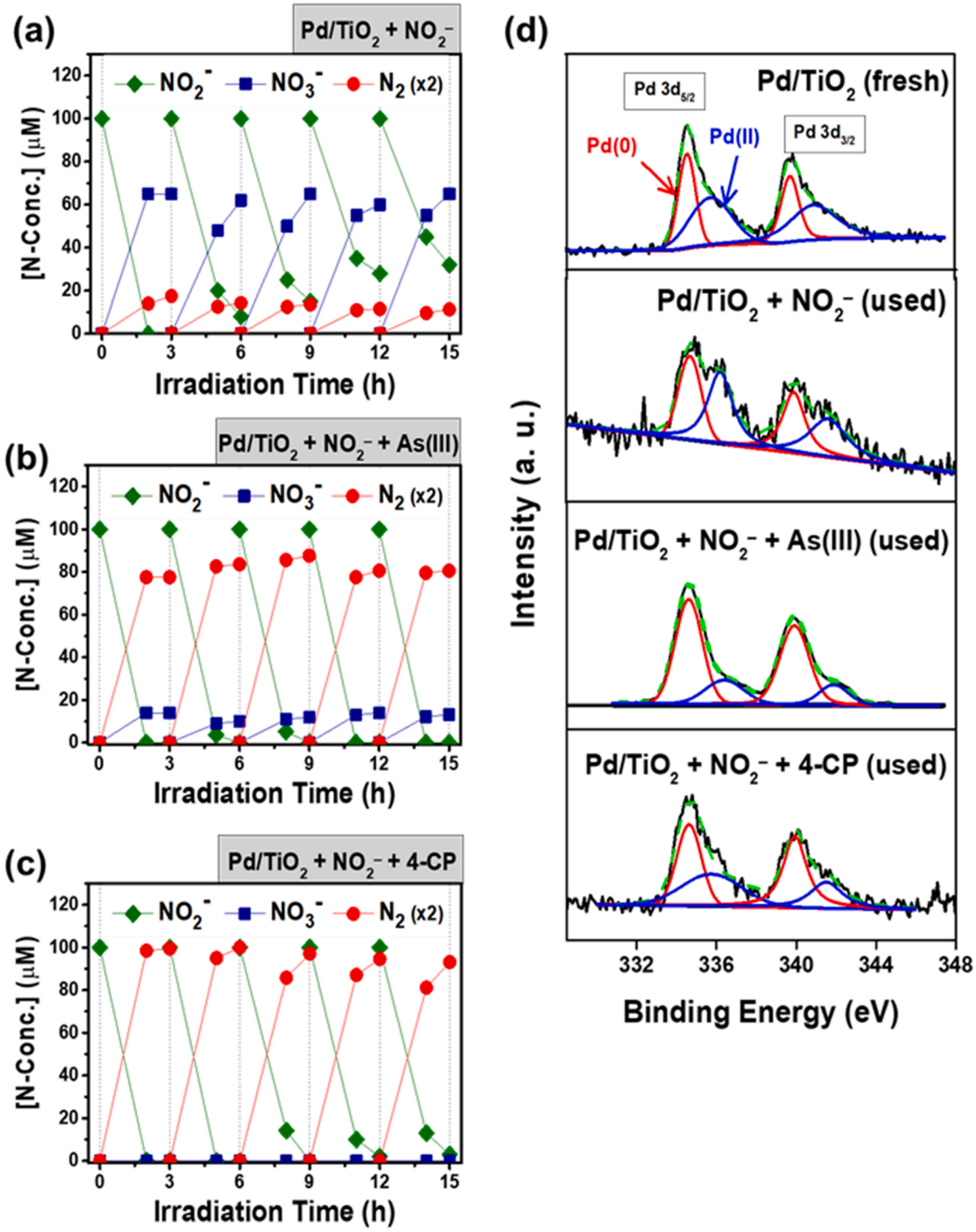

Fig. 11. The repeated tests for the photocatalytic conversion of nitrite and the concurrent generation of nitrate and N_2 on Pd/TiO_2 in the (a) absence and presence of (b) As(III) and (c) 4-CP. (d) X-ray photoelectron spectra (XPS) of Pd 3d bands in Pd/TiO_2 before and after 5 repeated photoreactions. ([catalyst] = 0.5 g/L; Pd content: 1 wt%; $[NO_2^-]_0 = 100$ μM; $[4\text{-CP}]_0 = [As(III)]_0 = 300$ μM; pH = 5.3–6.1 (not adjusted); initially Ar-purged (de-aerated suspension); $\lambda > 320$ nm).

frequency of 9.42 GHz, modulation frequency of 100 kHz, modulation amplitude of 2.0 G.

2.4. Photoelectrochemical measurements

Photoelectrochemical (PEC) experiments were performed using a conventional three-electrode potentiostat setup connected to a computer-controlled potentiostat-galvanostat (Gamry Instruments Reference 600). The reactor for electrochemical experiments consisted of a catalyst-coated transparent conducting substrate ($F:SnO_2$ (FTO) Pilkington, 15 Ω/square), a graphite rod, and a Ag/AgCl electrode as a working, a counter, and a reference electrode, respectively, in aqueous electrolyte of 0.1 M $NaClO_4$ under UV irradiation ($\lambda > 320$ nm). Ar gas was continuously purged into the reactor. The catalyst-coated electrodes were prepared by a Dr. Blade method. Catalyst powder (0.15 g) was ground for 15 min with 1 mL ethanol. The mixture was annexed onto the

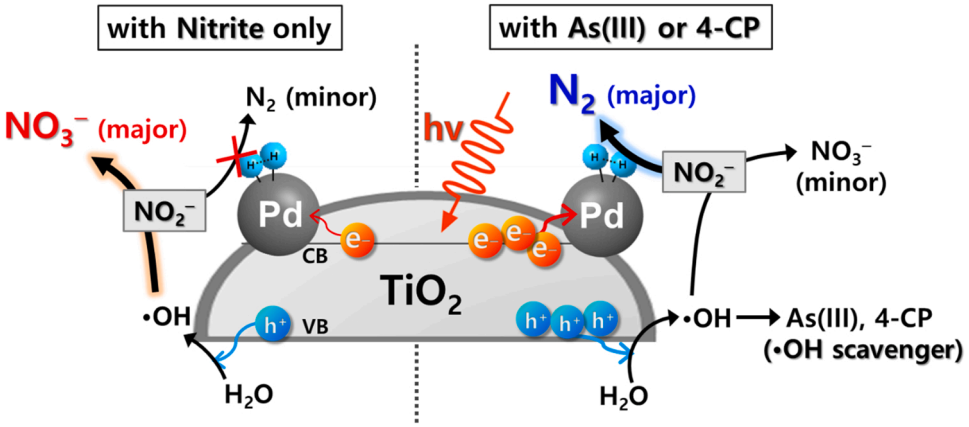

Scheme 1. The different nitrite conversion pathways on Pd/TiO_2 with or without aquatic pollutants.

FTO glass (Pilkington, TEC8) with an electrode area of 1.5 cm × 1 cm. The electrode was annealed in a muffle furnace at 450 °C for an hour with a ramping rate of 5 °C per min under ambient atmosphere.

3. Results and discussion

3.1. Photocatalytic conversion of NO_2^- on Pd/TiO_2

The photocatalyst samples of M/TiO_2 loaded with various metals (M, 1 wt%) were prepared and tested for their photoactivities for nitrite removal under anoxic condition, and all experiments were performed in the absence of externally added electron donors (Fig. 1a). Among the diverse M/TiO_2 systems, Pd/TiO_2 showed the most desired activity than others as it exhibited the highest removal of NO_2^-, the lowest production of NO_3^-, and the negligible production of NH_4^+, which might be attributed to the superior activities of Pd for high hydrogen spill-over and high adsorption of nitrite compared to other noble metals [27,28]. By contrast, bare TiO_2 and other M/TiO_2 (Ni, Pt, Cu, Ag, and Au/TiO_2) showed that most of removed nitrite was converted to nitrate and ammonium only with little sign of N_2 formation. On the other hand, it is interesting to note that a much smaller fraction of the removed nitrite was converted to NO_3^- and NH_4^+ in the presence of As(III), which might be ascribed to the enhanced production of N_2 (Fig. 1b). Although this As (III)-enhanced N-mass deficit (*i.e.,* enhanced N_2 production) was observed for all M/TiO_2 systems (Ni, Pd, Pt, Cu, Ag, and Au/TiO_2), Pd/TiO_2 exhibited the highest N-mass deficit, which implies that Pd/TiO_2 should be the most active for N_2 production. For this reason, we selected Pd/TiO_2 as a model photocatalyst for the further investigations of the conversion of nitrite.

To analyze the structure of the deposited Pd on TiO_2, HRTEM (high-resolution TEM) images and the elemental mapping images obtained with EFTEM (energy-filtered TEM) of Pd/TiO_2 are shown in Fig. 2a. The average size of Pd nanoparticles is approximately 3.2 nm. The elemental mapping analysis shows that Pd nanoparticles are well deposited on the supporting TiO_2 particles. To find the optimum catalyst condition for the highest conversion of NO_2^- and the highest N_2 selectivity, the loading of Pd on TiO_2 was varied (Fig. 2b). The N_2 yield was enhanced as the Pd content increased from 0 to 1 wt%. Further increase of Pd loading was not effective and slightly increased NO_3^- generation. As a result, the optimal catalyst composition for the maximal N_2 yield was determined at 1 wt% Pd loading.

3.2. NO_2^- conversion coupled with pollutants oxidation

The co-presence effects of several aquatic pollutants on the photocatalytic conversion of NO_2^- were tested and compared for the product distribution and the N_2 selectivity (*see* Fig. 3). The following aquatic pollutants were selected as model pollutants: As(III), phenol, 4-chlorophenol (4-CP), 4-nitrophenol (4-NP), bisphenol A (BPA), acetic acid, ascorbic acid, nitrobenzene (NB), which should serve as a scavenger of VB holes or OH radicals during photocatalysis [36,37]. Regardless of the type of pollutants, the N_2 selectivity was highly enhanced and the photocatalytic oxidation of NO_2^- to NO_3^- is significantly hindered in the presence of pollutants. Without aquatic pollutants, 62% of the removed NO_2^- was oxidized to NO_3^- in the irradiated Pd/TiO_2 suspension (Fig. 4a). On the other hand, when As(III) or 4-CP was added as a model inorganic and organic pollutant, the production of NO_3^- was markedly suppressed but the N_2 production was greatly enhanced instead (Fig. 4b and c). No other gas products (H_2 and O_2) were generated during the photoreaction. The near quantitative conversion of nitrite to N_2 was maintained even when the initial concentration of nitrite increased from 100 to 1000 μM (*see* Fig. 5). The photocatalytic production of NO_3^- was further suppressed when the initial concentration of As(III) and 4-CP increased from 100 μM to 300 μM (Fig. 6a). The photocatalytic removal of nitrite was accompanied by the concurrent removal of As(III) and 4-CP as shown in Fig. 6b and c. As(III) was oxidized to As(V) and 4-CP was degraded with the concurrent generation of chloride ions while NO_2^- was reduced to N_2. In this case, Pd/TiO_2 plays the dual roles of reducing nitrite and oxidizing additional pollutants (As(III) and 4-CP).

Most experiments in this study were conducted under anoxic conditions with 30 min Ar purging prior to irradiation and high N_2 selectivity was obtained in anoxic condition. Interestingly, when the mixed gas of Ar–H_2 (95: 5) was continuously purged into the reactor under dark condition, NO_2^- was completely removed in 1 h with generating negligible NO_3^- (Fig. 7a). This clearly indicates that photogenerated H_2 should be involved as an *in-situ* reductant for nitrite conversion. The photoreduction of NO_2^- coupled with As(III) oxidation was further investigated under different gas purging conditions (Fig. 7b). In the O_2-saturated condition, the photooxidation of NO_2^- generates NO_3^- whereas the production of NO_3^- was greatly suppressed under the Ar-purged condition. This implies that O_2 is actively involved in the oxidation of NO_2^- to NO_3^-. Furthermore, N_2 was produced only under Ar-purged condition (*see* the inset of Fig. 7b). The generation of NH_4^+ was negligible in all cases. The control tests showed that Pd/TiO_2 has no activity for the photocatalytic conversion of NO_3^- and NH_4^+ (data not shown), which is in accordance with the fact that Pd is completely inactive for nitrate conversion due to its weak adsorption affinity for nitrate [28,38].

The photocatalytic conversion of nitrite in the anoxic condition is closely coupled with the photocatalytic generation of H_2 as shown in Fig. 8. H_2 was produced on Pd/TiO_2 photocatalyst in the absence of NO_2^- but not in the presence of nitrite. This implies either that the *in-situ* generated H_2 was immediately consumed by NO_2^- or that the production of H_2 was inhibited because NO_2^- is a stronger electron acceptor than proton. The photocatalytic removal of nitrite in the Ar-purged solution

generated the sub-stoichiometric amount of nitrate, which implies the production of N_2 (Fig. 7a). On the other hand, Pd/TiO_2 catalyst can remove nitrite completely with little generation of nitrate even in the dark condition when H_2 gas was introduced into the catalyst suspension. This clearly indicates that H_2 reacts with NO_2^- on Pd/TiO_2 catalyst to generate a stoichiometric amount of N_2. Therefore, the fact that no H_2 was produced on Pd/TiO_2 photocatalyst in the presence of nitrite should be ascribed to that *in-situ* generated H_2 is immediately consumed by NO_2^-.

3.3. The role of hydroxyl radical in NO_2^- oxidation

Nitrite can be oxidized by valence band holes or hydroxyl radicals in the photocatalytic system [39] (Eqs. 5–7).

$$3NO_2^- + 3\ H_2O + 6\ h^+ \rightarrow 3NO_3^- + 6\ H^+ \quad (5)$$

$$\bullet OH + NO_2^- \rightarrow OH^- + NO_2\bullet \quad (6)$$

$$NO_2\bullet + NO_2\bullet + H_2O \rightarrow NO_3^- + NO_2^- + 2\ H^+ \quad (7)$$

To assess the role of OH radicals in NO_2^- oxidation, the photocatalytic activity tests were carried out in the presence of TBA (t-butyl alcohol) and EDTA (ethylenediaminetetraacetic acid) as a scavenger for hydroxyl radicals and holes, respectively (Fig. 9a) [40]. In the presence of TBA and EDTA, NO_3^- generation on Pd/TiO_2 was highly inhibited. The addition of As(III) and 4-CP as alternative scavengers exhibited the similar effect. The presence of organic and inorganic substrates that react rapidly with hydroxyl radicals inhibits the oxidation of NO_2^- while facilitating the reductive path leading to N_2. The production of •OH in aqueous Pd/TiO_2 suspension was confirmed by EPR spin-trapping technique (Fig. 9b). The EPR signal assigned to the DMPO−OH adduct was detected on Pd/TiO_2 under light irradiation whereas the characteristic peaks were slightly decreased in the presence of NO_2^-. This indicates that nitrite reacts with OH radicals. The EPR peaks of DMPO−OH almost completely disappeared when As(III) or 4-CP was added, which reconfirms that •OH is rapidly consumed by these substrates with inhibiting the oxidation of NO_2^- to NO_3^- (*see* Fig. 9a).

3.4. Enhanced charge transfer on Pd/TiO_2

It is proposed that the oxidation of As(III) and the reduction of NO_2^- occur concurrently at adjacent sites on the surface of Pd. To investigate the impact of coexistence of nitrite and aquatic pollutants (4-CP and As(III)) on the charge recombination, the photocurrent that responses under bias potential was measured using the Pd/TiO_2-coated electrode. The photocurrent generation on the irradiated Pd/TiO_2 electrode with or without 4-CP and As(III) upon turning on/off the light was recorded as a function of time (Fig. 10). The photocurrent production was markedly enhanced when the pollutants (As(III) or 4-CP) were added. This indicates that the additional pollutants scavenge hole/•OH with making more CB electrons react with NO_2^-, which is consistent with the observation that the photoconversion of NO_2^- to N_2 was enhanced when coupled with the oxidation of As(III) or 4-CP in the irradiated Pd/TiO_2 suspension.

The stability and reusability of Pd/TiO_2 need to be confirmed for practical applications. The photocatalytic nitrite removal using Pd/TiO_2 was tested through multiple cycles in the presence and absence of aquatic pollutants (As(III) and 4-CP). The nitrite removal efficiency of Pd/TiO_2 was gradually reduced (Fig. 11a), which implies that the Pd surface was deactivated during photo irradiation probably due to the oxidation of Pd to PdO_x. On the other hand, in the presence of 4-CP or As(III), Pd/TiO_2 maintained the photocatalytic activity during the repeated cycles with producing more N_2 and suppressing the generation of nitrate (Fig. 11b and c). The XPS analysis of the catalyst surface clearly showed the change of Pd oxidation state before and after the photoreaction (Fig. 11d): the Pd band is composed of two peaks originated from Pd^0 at 340.6 and 335.2 eV and $Pd^{II}O$ at 341.6 and 336.2 eV [41]. The content of oxidized Pd species (Pd(II)) was increased after the photoreaction of nitrite on the Pd/TiO_2, which explains why the photocatalytic activity of Pd/TiO_2 is reduced after repeated uses. However, in the presence of 4-CP or As(III), the content of $Pd^{II}O$ was not increased after the photoreaction, which indicates that the oxidation of Pd surface is inhibited as the added pollutants scavenge hole/•OH with keeping the Pd surface from being oxidized.

4. Conclusions

The conversion of NO_2^- is an essential step in the nitrogen cycle. The photocatalytic conversion behavior of NO_2^- is much less studied, compared to that of NO_3^-. Various mono/bimetallic cocatalyst-loaded semiconductors have been investigated but they either need chemical reductants or suffer from low conversion efficiency and low N_2 selectivity. This work demonstrated that the photocatalytic conversions of NO_2^- to N_2 in aqueous suspension of Pd/TiO_2 is markedly enhanced in the presence of aquatic pollutants that inhibit the oxidation of NO_2^- to NO_3^- by scavenging OH radicals/holes. As a result of hindered nitrite oxidation, more nitrite ions can be reductively transformed to N_2 on Pd/TiO_2. The nitrite reduction mechanisms on Pd/TiO_2 with and without aquatic pollutants are illustrated in Scheme 1. During the photoreaction on Pd/TiO_2 in the absence of additional aquatic pollutants, NO_2^- can react with either photogenerated electron or •OH/hole, which leads to the generation of NO_3^- as a major oxidation product and N_2 as a minor reduction product, respectively. When additional aquatic pollutants are present, they can scavenge photogenerated •OH/hole with suppressing the oxidation of NO_2^- but enhancing the reductive conversion to N_2 on the contrary. The effective hole scavenging by the pollutants not only enhances the N_2 selectivity but also keeps the Pd catalyst from being oxidized during photocatalysis. Pd nanoparticles acting as an electron reservoir effectively transfer the CB electrons to protons with producing H_2, which is immediately used as an *in-situ* reductant of nitrite in this photocatalytic system. The present study provides a basic strategy that can be utilized for the further development of practical photocatalytic denitrification systems that couple the reduction of nitrite and the photooxidation of various aquatic pollutants.

CRediT authorship contribution statement

Shinbi Lee: Formal analysis, Investigation, Visualization, Writing – original draft, **Yoojin Lee**: Formal analysis, Investigation, Writing – original draft, **Wonyong Choi**: Conceptualization, Methodology, Validation, Supervision, Resources, Data curation, Writing – original draft, Writing – review & editing.

Declaration of Competing Interest

The authors declare that they have no known competing financial interests or personal relationships that could have appeared to influence the work reported in this paper.

Data Availability

Data will be made available on request.

Acknowledgements

This research was financially supported by the Leading Researcher Program (NRF-2020R1A3B2079953), which was funded by the Korea government (MSIT) through the National Research Foundation of Korea (NRF).

References

[1] C. Ye, H. Gao, N. Zhang, X. Zhou, Photolysis of nitric acid and nitrate on natural and artificial surfaces, Environ. Sci. Technol. 50 (2016) 3530–3536.
[2] Q.R. Shen, W. Ran, Z.H. Cao, Mechanisms of nitrite accumulation occurring in soilnitrification, Chemosphere 50 (2003) 747–753.
[3] N. Lehnert, B.W. Musselman, L.C. Seefeldt, Grand challenges in the nitrogen cycle, Chem. Soc. Rev. 50 (2021) 3640–3646.
[4] K. Flores, G.A. Cerrón-Calle, C. Valdes, A. Atrashkevich, A. Castillo, H. Morales, J. G. Parsons, S. Garcia-Segura, J.L. Gardea-Torresdey, Outlining key perspectives for the advancement of electrocatalytic remediation of nitrate from polluted waters, ACS EST Engg. 2 (2022) 746–768.
[5] D. Zhang, M. Li, Y. Yang, H. Yu, F. Xiao, C. Mao, J. Huang, Y. Yu, Y. Wang, B. Wu, C. Wang, L. Shu, Z. He, Q. Yan, Nitrite and nitrate reduction drive sediment microbial nitrogen cycling in a eutrophic lake, Water Res. 220 (2022), 118637.
[6] K. Cosby, K.S. Partovi, J.H. Crawford, R.P. Patel, C.D. Reiter, S. Martyr, B.K. Yang, M.A. Waclawiw, G. Zalos, X. Xu, K.T. Huang, H. Shields, D.B. Kim-Shapiro, A. N. Schechter, R.O. Cannon III, M.T. Gladwin, Nitrite reduction to nitric oxide by deoxyhemoglobin vasodilates the human circulation, Nat. Med. 9 (2003) 1498–1505.
[7] E.Å. Jansson, L. Huang, R. Malkey, M. Govoni, C. Nihlén, A. Olsson, M. Stensdotter, J. Petersson, L. Holm, E. Weitzberg, J.O. Lundberg, A mammalian functional nitrate reductase that regulates nitrite and nitric oxide homeostasis, Nat. Chem. Biol. 4 (2008) 411–417.
[8] J. Martínez, A. Ortiz, I. Ortiz, GDF-15 plasma levels in chronic obstructive pulmonary disease are associated with subclinical coronary artery disease, Appl. Catal. B Environ. 207 (2017) 42–59.
[9] M. Duca, M.T.M. Koper, Powering denitrification: the perspectives of electrocatalytic nitrate reduction, Energy Environ. Sci. 65 (2012) 9726–9742.
[10] V. Mateju, S. Cizinska, J. Krejci, T. Janoch, Biological water denitrification—a review, Enzym. Microb. Technol. 14 (1992) 170–183.
[11] V. Höller, K. Rådevik, I. Yuranov, L. Kiwi-Minsker, A. Renken, Reduction of nitrite-ions in water over Pd-supported on structured fibrous materials, Appl. Catal. B Environ. 32 (2001) 143–150.
[12] M.S. Koo, H. Kim, K.E. Lee, W. Choi, ACS EST Engg. 2 (2020) 228–238.
[13] X. Zhang, Wang, Y. Wang, Y. Guo, X. Xie, Y. Yu, B. Zhang, Recent advances in electrocatalytic nitrite reduction, Chem. Commun. 58 (2022) 2777–2787.
[14] W. Gao, N. Guan, J. Chen, X. Guan, R. Jin, H. Zeng, Z. Liu, F. Zhang, Titania supported Pd-Cu bimetallic catalyst for the reduction of nitrate in drinking water, Appl. Catal. B Environ. 46 (2003) 341–351.
[15] Y. Li, Y.K. Go, H. Ooka, D. He, F. Jin, S.H. Kim, R. Nakamura, Enzyme mimetic active intermediates for nitrate reduction in neutral aqueous media, Angew. Chem., Int. Ed. 132 (2020) 9831–9837.
[16] O. Brylev, M. Sarrazin, L. Roué, D. Bélanger, Nitrate and nitrite electrocatalytic reduction on Rh-modified pyrolytic graphite electrodes, Electrochim. Acta 52 (2007) 6237–6247.
[17] M. Duca, B. van der Klugt, M.A. Hasnat, M. Machida, M.T.M. Koper, Electrocatalytic reduction of nitrite on a polycrystalline rhodium electrode, J. Catal. 275 (2010) 61–69.
[18] H. Xu, Y. Ma, J. Chen, W.-X. Zhang, J. Yang, Electrocatalytic reduction of nitrate - a step towards a sustainable nitrogen cycle, Chem. Soc. Rev. 51 (2022) 2710–2758.
[19] C. Park, H. Kwak, G. –H. Moon, W. Kim, Biomimetic photocatalysts for the conversion of aqueous- and gas-phase nitrogen species to molecular nitrogenviadenitrification and ammonia oxidation, J. Mater. Chem. A 9 (2021) 19179–19205.
[20] X. Zhao, G. Zhang, Z. Zhang, TiO(2)-based catalysts for photocatalytic reduction of aqueous oxyanions: State-of-the-art and future prospects, Environ. Int. 136 (2020), 105453.
[21] S. –R. Huang, P. –J. Huang, Visible-light driven graphene oxide/titanium dioxide hydrogels for photocatalytic reduction of nitrite, J. Environ. Chem. Eng. 10 (2022), 106902.
[22] J.E. Silveira, A.R. Ribeiro, J. Carbajo, The photocatalytic reduction of NO(3)(-) to N (2) with ilmenite (FeTiO3): Effects of groundwater matrix, Water Res 200 (2021), 117250.
[23] H. Shi, C. Li, L. Wang, W. Wang, Selective reduction of nitrate into N(2) by novel Z-scheme NH(2)-MIL-101(Fe)/BiVO(4) heterojunction with enhanced photocatalytic activity, J. Hazard. Mater. 424 (2022), 127711.
[24] F. Zhang, Y. Pi, J. Cui, Y. Yang, X. Zhang, N. Guan, Unexpected selective photocatalytic reduction of nitrite to nitrogen on silver-doped titanium dioxide, J. Phys. Chem. C. 111 (2007) 3756–3761.
[25] H.-T. Ren, S.-Y. Jia, J.-J. Zou, S.-H. Wu, X. Han, The activation of protein homeostasis protective mechanisms perhaps is not responsible for lifespan extension caused by deficiencies of mitochondrial proteins in C. elegans, Appl. Catal. B Environ. 176–177 (2015) 53–61.
[26] H.O. Tugaoen, S. Garcia-Segura, K. Hristovski, P. Westerhoff, Challenges in photocatalytic reduction of nitrate as a water treatment technology, Sci. Total Environ. 599–600 (2017) 1524–1551.
[27] U. Prüsse, K. Vorlop, Supported bimetallic palladium catalysts for water-phase nitrate reduction, J. Mol. Catal. A Chem. 173 (2001) 313–318.
[28] H. Shin, S. Jung, S. Bae, W. Lee, H. Kim, Nitrite reduction mechanism on a Pd surface, Environ. Sci. Technol. 48 (2014) 12768–12774.
[29] D. Shuai, J.K. Choe, J.R. Shapley, C.J. Werth, Enhanced activity and selectivity of carbon nanofiber supported Pd catalysts for nitrite reduction, Environ. Sci. Technol. 46 (2012) 2847–2855.
[30] H. Kominami, H. Gekko, K. Hashimoto, Photocatalytic disproportionation of nitrite to dinitrogen and nitrate in an aqueous suspension of metal-loaded titanium(IV) oxide nanoparticles, Phys. Chem. Chem. Phys. 12 (2010) 15423–15427.
[31] H. Gekko, K. Hashimoto, H. Kominami, Photocatalytic reduction of nitrite to dinitrogen in aqueous suspensions of metal-loaded titanium(IV) oxide in the presence of a hole scavenger: an ensemble effect of silver and palladium co-catalysts, Phys. Chem. Chem. Phys. 14 (2012) 7965–7970.
[32] S. Lee, S. Kim, C. Park, W. Kim, S. Ryu, W. Choi, Solar denitrification coupled within situwater splitting, Energy Environ. Sci. 14 (2021) 4437–4450.
[33] A.M. Perez-Coronado, L. Calvo, J.A. Baeza, J. Palomar, L. Lefferts, J.J. Rodriguez, M.A. Gilarranz, Selective reduction of nitrite to nitrogen with carbon-supported Pd–AOT nanoparticles, Ind. Eng. Chem. Res. 56 (2017) 11745–11754.
[34] H. Li, S. Guo, K. Shin, M.S. Wong, G. Henkelman, Design of a Pd–Au nitrite reduction catalyst by identifying and optimizing active ensembles, ACS Catal. 9 (2019) 7957–7966.
[35] V. Lenoble, V. Deluchat, B. Serpaud, J.C. Bollinger, Arsenite oxidation and arsenate determination by the molybdene blue method, Talanta 61 (2003) 267–276.
[36] C. Kim, S. Chae, Y. Park, W. Choi, Synergistic coupling of Fe2O3and carbon paper that enables photocatalytic mineralization of organic contaminants in the absence of chemical oxidants under visible light, ACS EST Engg. 2 (2022) 232–241.
[37] J.Y. Hwang, G. –H. Moon, B. Kim, T. Tachikawa, T. Majima, S. Hong, K. Cho, W. Kim, W. Choi, Crystal phase-dependent generation of mobile OH radicals on TiO2: Revisiting the photocatalytic oxidation mechanism of anatase and rutile, Appl. Catal. B Environ. 286 (2021), 119905.
[38] F. Deganello, L.F. Liotta, A. Macaluso, A.M. Venezia, G. Deganello, Catalytic reduction of nitrates and nitrites in water solution on pumice-supported Pd–Cu catalysts, Appl. Catal. B Environ. 24 (2000) 265–273.
[39] D.-h Kim, J. Lee, J. Ryu, K. Kim, W. Choi, Arsenite oxidation initiated by the UV photolysis of nitrite and nitrate, Environ. Sci. Technol. 48 (2014) 4030–4037.
[40] T. Li, A. Abdelhaleem, W. Chu, S. Pu, F. Qi, J. Zou, S-doped TiO2 photocatalyst for visible LED mediated oxone activation: kinetics and mechanism study for the photocatalytic degradation of pyrimethanil fungicide, Chem. Eng. J. 411 (2021), 128450.
[41] A. Serov, T. Asset, M. Padilla, I. Matanovic, U. Martinez, A. Roy, K. Artyushkova, M. Chatenet, F. Maillard, D. Bayer, C. Cremers, P. Atanassov, Highly-active Pd–Cu electrocatalysts for oxidation of ubiquitous oxygenated fuels, Appl. Catal. B Environ. 191 (2016) 76–85.